Universal features of the equation of state of solids

1989 J. Phys.: Condens. Matter 1 1941

(http://iopscience.iop.org/0953-8984/1/11/002)

J. Phys.: Condens. Matter **1** (1989) 1941–1963. Printed in the UK

Universal features of the equation of state of solids

Pascal Vinet†, James H Rose‡, John Ferrante§ and John R Smith‖

† Laboratoire de Technologie des Surfaces, Ecole Centrale de Lyon, BP 163, 69131 Ecully Cedex, France

‡ Ames Laboratory, Iowa State University, Ames, Iowa 50011, USA

§ National Aeronautics and Space Administration, Lewis Research Center, Cleveland, Ohio 44135, USA

‖ Physics Department, General Motors Research Laboratories, Warren, Michigan 48090, USA

Received 19 April 1988, in final form 20 September 1988

Abstract. A study of the energetics of solids leads to the conclusion that the equation of state for *all* classes of solids in compression can be expressed in terms of a universal function. The form of this universal function is determined by scaling experimental compression data for measured isotherms of a wide variety of solids. The equation of state is thus known (in the absence of phase transitions), if zero-pressure volume and isothermal compression and its pressure derivative are known. The discovery described in this paper has two immediate consequences: first, despite the well known differences in the microscopic energetics of the various classes of solids, there is a single equation of state for all classes in compression; and second, a new method is provided for analysing measured isotherms and extrapolating high-pressure data from low-pressure (e.g. acoustic) data.

1. Introduction

The equation of state (EOS) of a solid (P, V, T relation) is fundamentally important in basic and applied science [1–7]. It depends on the nature of the interatomic interactions and thus provides a test of fundamental solid state theories. At the same time, it can be used to determine thermodynamic properties.

Many analytic, semiempirical relations have been proposed to describe the EOS. Such proposals have been based on two different approaches. The first attempts to find reliable methods of curve fitting using, for example, finite stress–strain relations. This approach has been moderately successful in finding fitting forms (such as the Birch–Murnaghan equation [8]) and describes the P, V, T data for a wide variety of solids. The second approach has been to propose models based on the rather different energetics of the various classes of solids. For example, the EOS of alkali halides has been described by the Born–Mayer potential, while the EOS of rare-gas solids has been modeled by the Buckingham potential [9]. Consequently the second approach had led to a plethora of more or less complicated functional forms. Both approaches are extensively reviewed in [1–5].

In this paper following the second approach we will show that this plethora of forms is not necessary and that a single form will suffice. This study relies on the recent discovery of a universal, scaled, energy relation for covalent and metallic solids. We will show

0953-8984/89/111941 + 23 $02.50

that, despite the rather different features of their energetics, the EOS in compression of *all* classes of solids (metallic, covalent, ionic, van der Waals) can, in the absence of phase transitions, be described by a scaled, universal function. Consequently, the two way of describing the EOS semi-empirically have culminated in a single relationship.

The form of the universal relation is not assumed *a priori*, but is discovered by analysis of energetics. The form is then determined by plotting experimental isotherms in a simple, model-free way. The resulting curves have the same shape and in fact are linear. Consequently, the EOS can be represented by a particularly simple, functional form. Alternatively, the form of the EOS can be derived from the universal energy relations. Interested readers can find a brief report of this derivation in [10]. The remaining part of this paper is divided into five sections. Here we emphasise an empirical approach. The data required as input are the zero-pressure volume, $V_0(T)$, isothermal bulk modulus, $B_0(T)$, and pressure derivative of the isothermal bulk modulus, $B_0'(T) = (\partial B/\partial P)_{P=0,T}$. Here, T denotes the temperature, and B the isothermal bulk modulus at arbitrary P and T. We note that B_0 and B_0' can be determined by low-pressure acoustic experiments, while $V_0(T)$ is easily measured.

The discovery of a universal EOS for all classes of solids in compression stems from an ongoing study of universal features in the energetics of metals [11–19]. In § 2 we review these results and their consequences, previously reported, of a universal EOS for zero-temperature metals [15, 16]. In § 3 we provide theoretical arguments that the same universal form may be expected to describe the EOS of all other classes of solids at non-zero temperatures. Section 4 uses the results of § 2 to describe a model-free test of universality. This test is then applied to the measured isotherms of van der Waals, ionic, covalent, and metallic solids. Section 4 will appear to be repetitive since the same analysis must be performed for each class of solid in order to establish our hypothesis. Section 5 describes the significance of the test of universality used in § 4. Also, expressions are given for $B(V, T)$ and $(\partial^2 B/\partial P^2)_{P=0,T}$. Section 6 explores the use of the universal relation in the analysis of data. Various exceptional cases (such as data which includes a phase transition) are highlighted. Finally, the paper is concluded with a summary.

2. Review of universality for EOS of metals

Recently it has been shown that the isotherm EOS of metals has a simple, universal form [15, 16]. This results from the fact that, for metallic sytems, the $T = 0$ binding energy–distance relation can be described to good accuracy by [13, 14]

$$E(a) = \Delta E\, E^*(a^*). \tag{2.1}$$

Here $E(a)$ is the binding energy per atom, ΔE scales the energy, a measures the separation between atoms, and a^* is a scaled separation,

$$a^* = (a - a_0)/l \tag{2.2}$$

where a_0 is the equilibrium separation between atoms, and l is the scaling length. Equation (2.1) has been shown to hold for the adhesion of two metallic half-spaces [11, 18, 19], chemisorption of gas atoms on metal surfaces [12], and in particular for cohesion of bulk metals [13, 14]. It has even been used to describe nuclear interaction potentials and to predict the equation of state of nuclear matter [20].

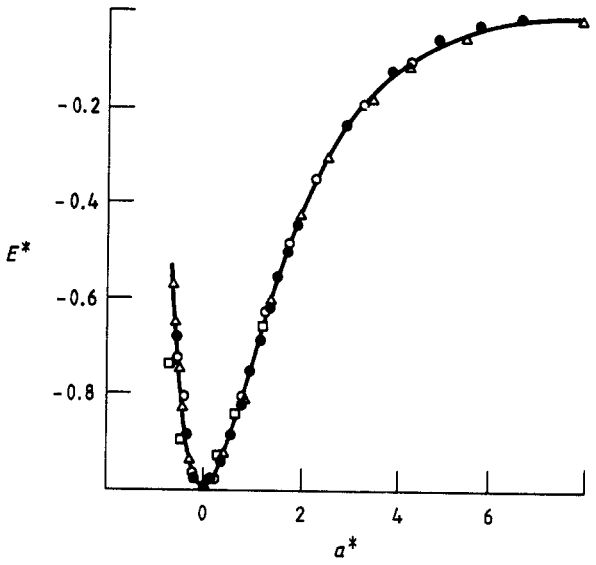

Figure 1. Universal binding energy relation—scaled binding energy (E^*) versus scaled separation (a^*)—for diatomics (●, H_2^+ (molecule)), adhesion (○, Al–Zn (interface)), chemisorption (□, oxygen (chemisorbed)), and cohesion (△, Mo (bulk)).

Figures 1 and 2 illustrate the universal shape of the binding energy distance curves. Figure 1 (taken from [13]) documents this result for several representative cases: (1) H_{2^+}, a diatomic molecule; (2) oxygen chemisorbed on jellium; (3) bimetallic adhesion of Al and Zn; and (4) cohesion of bulk Mo. Figure 2 (also taken from [13]) shows the cohesive energy as a function of the scaled lattice constant for a variety of metals. The full line in these figures is given as an aid to the eye and is expressed below by equation (2.12).

For the rest of this section, we will consider the cohesion of bulk metals; that is, we use equations (2.1) and (2.2) to describe the energetics of bonding of a bulk metal as a

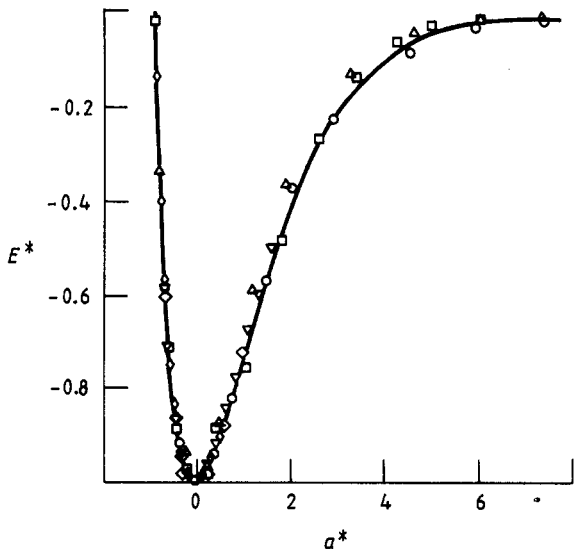

Figure 2. Universal binding energy relation—scaled binding energy (E^*) versus scaled separation (a^*)—for cohesion of metals ranging from simple metals to transition metals: ○, Mo; □, K; △, Cu; ◇, Ba; ◊, Sm^{2+}; ▽, Sm^{3+}.

function of the scaled lattice constant *expanded of compressed*. From here on, ΔE is the zero-pressure binding energy per atom (cohesive energy) and

$$a^* = (r_{WS} - r_{WSE})/l. \tag{2.3}$$

Here r_{WS} is the average Wigner–Seitz radius and is given by $V = 4\pi r_{WS}^3$, where V is the specific volume per atom—the zero-pressure value of r_{WS} is denoted by r_{WSE}. The length scale l is defined to be

$$l = [\Delta E/(\mathrm{d}^2E/\mathrm{d}a^2)_0]^{1/2} \tag{2.4}$$

and can be rewritten conveniently as

$$l = (\Delta E/12\pi r_{WSE} B_0)^{1/2}. \tag{2.5}$$

The zero-temperature, pressure–volume (P, V) curves of metals have been computed from (2.1), (2.3), and (2.5) and compared with experiment. Good agreement was obtained, as discussed in [15–17]. We review the derivation below. First, at $T = 0$ we write

$$P = -\partial E/\partial V. \tag{2.6}$$

Using the universal form for the energy, we obtain

$$P = -(\Delta E/4\pi r_{WSE} B_0)E^{*\prime}(a^*). \tag{2.7}$$

The prime indicates the derivative with respect to the argument. Just as E^* is a scaled energy, $E^{*\prime}$ is a scaled force. By Hooke's law, we may expect $E^{*\prime}$ to be proportional to a^* for small a^*. Consequently, it is convenient to write

$$E^{*\prime}(a^*) = a^* G^*(a^*). \tag{2.8}$$

Here $G^*(a^*)$ is a new universal function defined by (2.8) which describes the deviations from linearity in the universal force expression.

From equations (2.5), (2.7), and (2.8), one can give an expression for G^* explicitly in terms of the measured isotherms

$$G(a^*) = -(V/V_0)^{2/3} P(V)/3B_0[1 - (V/V_0)^{1/3}]. \tag{2.9}$$

A second, somewhat more convenient function $H(x)$ can also be introduced by

$$H(x) \equiv -B_0 G^*(a^*). \tag{2.10}$$

Here $x = (V/V_0)^{1/3}$. Rewriting (2.9) in terms of these definitions yields

$$H(x) = x^2 P(x)/3(1 - x). \tag{2.11}$$

Once universality is assumed (equation (2.1)), it follows that, to this approximation, plots of $H(x)$ versus x *must* have the same shape for all metals.

The results until now followed from the assumption that the energetics could be described by some universal function, $E^*(a^*)$. We have not had to specify the form of $E^*(a^*)$ in deriving (2.9) and (2.11). However, some further progress can be made by using an approximation for E^* known to be accurate for metals:

$$E^*(a^*) \simeq (1 + a^*)e^{-a^*}. \tag{2.12}$$

One finds that $G^*(a^*) = -\exp(-a^*)$. If this result is used in (2.10), one finds

$$\ln H(x) \simeq \ln B_0 + \eta(1 - x) \tag{2.13}$$

where $\eta = r_{WSE}/l$ is a constant. Equation (2.13) implies that plots of $\ln H(x)$ versus $1 - x$ should be nearly linear. The intercept is $\ln B_0$ and the slope is η.

Equation (2.12) allows us to approximate the P,V curve as

$$P = [3B_0(1 - x)/x^2] \exp[\eta(1 - x)]. \tag{2.14}$$

The bulk modulus and its pressure derivative can be computed from (2.14). The result fixes η in terms of B_0' as

$$\eta = \tfrac{3}{2}(B_0' - 1). \tag{2.15}$$

Note that in previous papers we have denoted B_0' as $(\partial B/\partial P)_{T,P=0}$.

3. Other classes of solids and non-zero temperatures

It was shown in [15] and [16] that the zero-temperature equations of state for a variety of metals are accurately described by (2.14). Hence plots of ln $H(x)$ versus $1 - x$ should be found to be straight lines. In this section we argue that: (i) this result generalises to other classes of solids and to finite temperatures, and (ii) equations of state for solids can be usefully described by a universal function.

On the face of it, it seems implausible that isothermal P, V curves for ionic, covalent, metallic, and van der Waals solids would be the same. The energetics of these solids are rather different. For example, in metals the attractive force between atoms is due primarily to electron overlap, whereas the attractive force between atoms in ionic crystals is the long-range Coulomb interaction, while van der Waals solids are held together by the long-range van der Waals interaction. Consequently, one might think that the isothermal P, V curves of each class of solids would have a distinct form. In fact, such reasoning has led to a myriad of semi-empirical formulas for the P, V curves of different classes of solids [1–5].

We will now examine the reasons why such a variety of fitting forms is not necessary. Consider an ionic crystal. The attraction is primarily provided by the long-range Coulomb force. The repulsive force that stabilises the crystal against collapse arises from the kinetic energy due to the overlap of the ion's electron clouds. The essential point is that this repulsive force varies much more rapidly than the attractive forces. Consequently, we have the following situation. In tension the long-range force contributes almost all of the *binding* energy. Note that the pressure is the derivative of the binding energy. However, although the short-range and long-range terms contribute nearly equally to the pressure near equilibrium, the rapid variation of the repulsive forces in the hard core implies that the short-range forces dominate the total pressure in compression.

Note that the observation of universality concerns the *shape* of the $H(x)$ curve, which in turn depends on the shape of the P, V curve. Since the repulsive and attractive contributions to P are equal at V_0, we may expect the rapidly growing repulsive contribution to dominate the shape of $H(x)$ for compression.

The same arguments apply more so to van der Waals solids, which have a filled shell interactions as do ionic solids. The long-range interaction is weaker in rare-gas solids than in ionic solids. Gordon and Kim [21] have found that, in the region of equilibrium, most of the inter-particle potential of rare-gas solids (including the attractive part) can be treated by the local-density electron-gas theory commonly used in the study of metals. Consequently, their energetics may be expected to be similar to those of metals in the region of compression.

The plausibility arguments just given rely on the assumption of zero temperature. At finite temperatures

$$P = -(\partial F(T, V)/\partial V)_T \tag{3.1}$$

where F is the Helmholtz free energy. By definition, the right-hand side of (3.1) is rewritten

$$P = -\mathrm{d}E(V)/\mathrm{d}V + P^*(T, V). \tag{3.2}$$

Here E is the $T = 0$ ground-state energy and P^* is defined as the thermal pressure. For high temperatures, $P^*(T, V)$ is not negligible. However, it is known in general that $P^*(T, V)$ is slowly varying function of V relative to $-\mathrm{d}E(V)/\mathrm{d}V$. Thus one might expect that the form of $-\mathrm{d}E/\mathrm{d}V$ and $P(T, V)$ would be similar; however, since $P^*(T, V)$ is not negligible, it will shift the equilibrium point so that the temperature dependence is contained in $V_0(T)$, $B_0(T)$ and $B_0'(T)$. That is, the shape of the isotherm as scaled by these three parameters is the same as the $T = 0$ isotherm.

To demonstrate this point quantitatively, we added a volume-independent $P^*(T)$ to pressure–volume data [22] for a caesium sufficient to increase or decrease $V_0(T)$ by up to 4%. This thermal volume change and corresponding change in thermal pressure is larger than one could actually encounter in solid caesium. Nevertheless, we found that the linearity of plots of $\ln H(V, T)$ versus $1 - (V/V_0(T))^{1/3}$ was virtually unchanged by the addition of $P^*(T)$. R-values, indicating quality of least-mean-square linear fit (see equation (4.1) below), varied from 0.999 95 for the original experimental data to 0.999 92 with the largest added $P^*(T)$. The effect of the added $P^*(T)$ was found in changes of corresponding $V_0(T)$, $B_0(T)$, and $(\partial B(T)/\partial P)_{T,P=0}$, however. For a more complete discussion of temperature effects, see [23].

4. Tests of universality

In this section we provide empirical evidence that the EOS of solids can be usefully described in terms of a single universal function. Since we are attempting to establish our hypothesis for a wide variety of experimental data, it will of necessity be repetitious. We start with equation (2.11) as the definition of $H(x)$. $H(x)$ can be evaluated entirely in terms of measurable quantities for any solid ($P(V, T)$ and $x(T) = (V(T)/V_0(T))^{1/3}$). The experimental isotherms are used to compute and plot $\ln H(x)$ versus $1 - x$ for a wide variety of solids. All of the resulting curves will be found to be straight lines to high accuracy. Consequently, the EOS is well described for all classes of solids by the universal expression given in (2.14).

We will plot $\ln H(x)$ versus $1 - x$ for each class of solids sequentially. In each case the resulting curves are fitted to a straight line. The fitting parameters $B_0(T)$ and $B_0'(T)$ are determined and reported. In addition, a confidence (correlation) factor for the quality of the data fitted to a line is reported.

Our results are grouped as follows. First, in § 4.1, we analyse solid H_2 and D_2. These data represent by far the greatest compressions available to us, the smallest value reported being 20% of the zero-pressure volume. Hence they provide a stringent test. In § 4.2 we discuss the compression of alkali metals, using the highly precise static-press measurements of [22, 24–30]. Next, shock wave data is analysed in § 4.3 for a variety of elemental metals and alloys. Ionic crystals are analysed in § 4.4, with special attention

paid to NaCl due to its use as a high-pressure standard. In § 4.5 rare-gas solids are analysed, using mainly the static-press data of [25, 29]. Finally, in § 4.6, results are presented for some polymers and amorphous solids.

We start by fitting $\ln H(x)$ versus $1 - x$ to a line. We use the correlation coefficient [31] to quantitatively define the degree of linearity. The definition of the correlation coefficient is

$$R = \left(\sum_{i=1}^{N} (y_i^{\mathrm{FIT}} - \bar{y})^2 \Big/ \sum_{i=1}^{N} (y_i^{\mathrm{DATA}} - \bar{y})^2 \right)^{1/2}. \tag{4.1}$$

Here y_i^{DATA} are the plotted values of $\ln H(x)$, $\bar{y}$ is the average of the N values of y_i^{DATA}, and y_i^{FIT} are the values taken from the fitting line. Note that the values of $1 - x$ are taken to be equally spaced. A correlation coefficient of unity indicates a perfect fit to a straight line.

As previously discussed, the linear fitting parameters provide an estimate for B_0 and B_0'. These values are reported for each substance analysed in this section. The reader is cautioned that these numbers are reported only to define our fits: they are sometimes taken from old and not always completely accurate P, V data. In particular, they should *not* be preferred to ultrasonic measurements of the same quantities. Deviations of B_0 and B_0' from ultrasonic measurements should, for the most part, reflect the approximate nature of our analysis and the quality of the data analysed.

Our selection of the data is idiosyncratic. We have for the most part preferred data that are part of either compendia or systematic studies of a family of elements. Studies of single elements have generally been omitted. Due to the volume of data, the entire set of the compendia of shock wave data has not been presented. Rather, we have selected about one-third of the elemental metals for presentation and have omitted a few of the alkali halides. The basis for selection was clarity of presentation since line crossings on the appropriate plot obscured their content. With few exceptions the data could be fitted by straight lines with high (>0.999) R-values.

4.1. Hydrogen and deuterium

Hydrogen is one of the most compressible elemental solids. The possible transition to a metallic state has prompted considerable effort to measure the P, V curve to high compressions. We make use of two experimental studies. The first, by Anderson and Swenson [29], reports the isotherm at 4.2 K to roughly 50% of the original volume. The second, by Van Straaten and co-workers [2], reports compressions to 20% of the original volume, also at 4.2 K. The resulting values of $\ln H$ are plotted versus $(1 - x)$ in figure 3. The dots correspond to the results of [29], while the crosses denote the results of [2]. As can be seen, both sets of data lie closely on a common straight line. From the data of [29], we infer $B_0 = 1.66 \times 10^8$ Pa for H_2 and $B_0 = 3.099 \times 10^8$ Pa for D_2; also $B_0' = 7.33$ for H_2 and $B_0' = 7.07$ for D_2. The correlation for the fit was $R = 0.9999$ for both D_2 and H_2. For data from [2] we find $B_0 = 1.62 \times 10^8$ Pa, $B_0' = 7.51$, and $R = 0.9999$ for H_2 while $B_0 = 3.019 \times 10^8$ Pa, $B_0' = 7.19$, and $R = 0.9997$ for D_2. Values of B_0, B_0', and R for hydrogen are listed in table 4 below, with the rare gas elements, for easy reference. The fact that the $\ln H(x)$ plot is a straight line over compression by a factor of five is a striking confirmation that equation (2.10) is not confined to metals.

4.2. Alkali metals

Recently Anderson and Swenson [22, 28] completed a systematic, precise study of the compression isotherms for Li, Na, K, Rb, and Cs. Tabular results for P, V were reported for pressures up to 20 kbar for temperatures of $T = 4.2$ K and $T = 295$ K (294 K for Li).

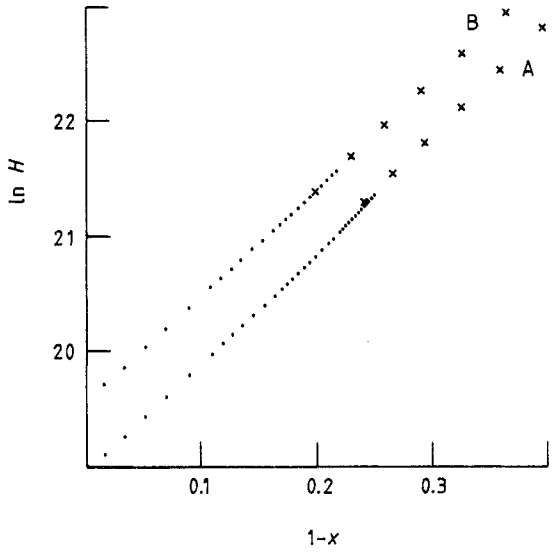

Figure 3. $\ln H$ (from equation (2.13)) versus $(1 - x)$ where $x = (V/V_0)^{1/3}$ for hydrogen (curve A) and deuterium (curve B) to high comperessions using data from [29] and [2] (×).

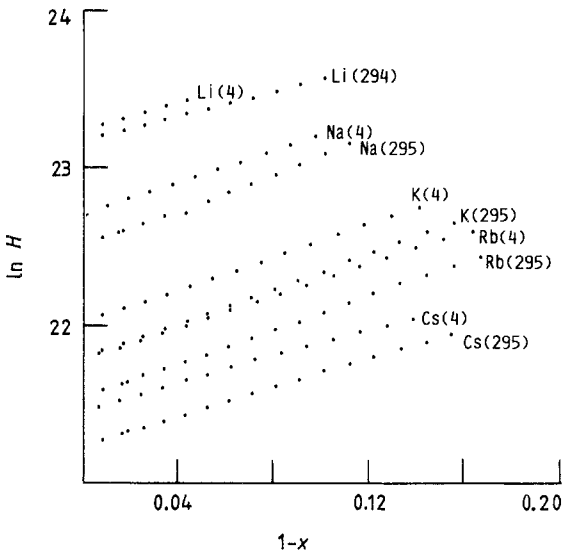

Figure 4. $\ln H$ (from equation (2.13)) versus $(1-x)$ where $x = (V/V_0)^{1/3}$ for simple metals at two temperatures (given in K against the element symbol) using data from [22] and [28].

The maximum compression for the alkalis was $V/V_0 \simeq 0.55$ for rubidium. For the other alkali metals, the maximum compression ranged to 0.85 for lithium.

Figure 4 shows plots of $\ln H(x)$ versus $1 - x$ for those elements. The data approximate straight lines in all cases, at 295 K as well as 4.12 K. Upon fitting the plots to a straight

Table 1. Curve-fitting parameters B_0 and B_0' from equation (2.13) for the alkali metals.

Material	B_0 (10^{10} Pa)	B_0'	R	$(V/V_0)_{min}$
Li (4.2 K)	1.25	3.8	0.9999	0.85
Li (294 K)	1.16	3.6	0.9999	0.72
Na (4.2 K)	0.72	4.4	0.9986	0.70
Na (295 K)	0.59	4.8	0.9879	0.70
K (4.2 K)	0.37	4.4	0.9999	0.60
K (295 K)	0.29	4.7	0.9999	0.60
Rb (4.2 K)	0.29	4.3	0.9998	0.55
Rb (295 K)	0.23	4.6	0.9999	0.55
Cs (4.2 K)	0.21	3.9	0.9994	0.60
Cs (295 K)	0.17	4.1	0.9997	0.60

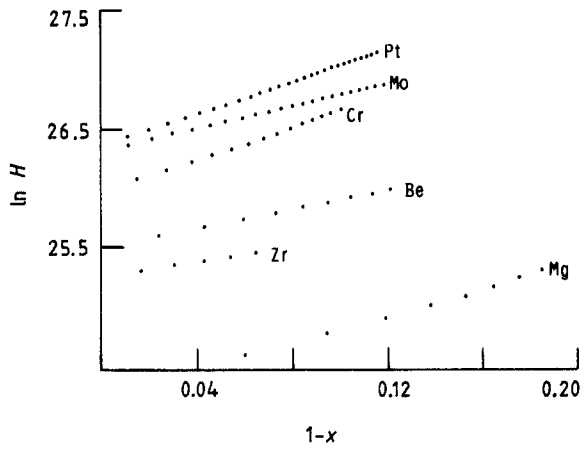

Figure 5. $\ln H$ (from equation (2.13)) versus $(1-x)$ where $x = (V/V_0)^{1/3}$ for several metals using the shock wave data of [32] and [33].

line, we obtain the values for B_0, B_0', and R given in table 1. The values of B_0 obtained in our analysis are in good agreement with those of [22] and [28]. Our values of B_0' appear to be larger by a small amount. Note as we asserted earlier the shapes of the isotherms are unaffected by temperature.

4.3. Other metals: shock wave data

Isothermal P, V curves have been estimated for many solids from shock wave measurements. Two useful compendia of these results have been given in [32, 33] as extrapolated to $T = 0$ K, and in [34] as extrapolated to 298 K.

Figures 5 and 6 show the results of plotting $\ln H(x)$ for a selection of the elemental metals and alloys reported by McQueen and co-workers (see [32], p 294 and especially p 53, [33]). In all cases, the linearity of $\ln H(x)$ is evident. Note that figure 6 supports the finding in [15] that universality applies to commercial alloys as well as pure elemental metals. Figure 7 reports $\ln H(x)$ for a selection of the shock wave data of [34] for metals. There is some scatter in the data at small compressions. The origin of this scatter is unknown but may be due to a lack of precision in the extrapolated results for low pressures. We note that, in those cases where scatter occurs, extracting B_0 and B_0' by a limiting process as $P \rightarrow 0$ would become difficult. However, this problem is minimised

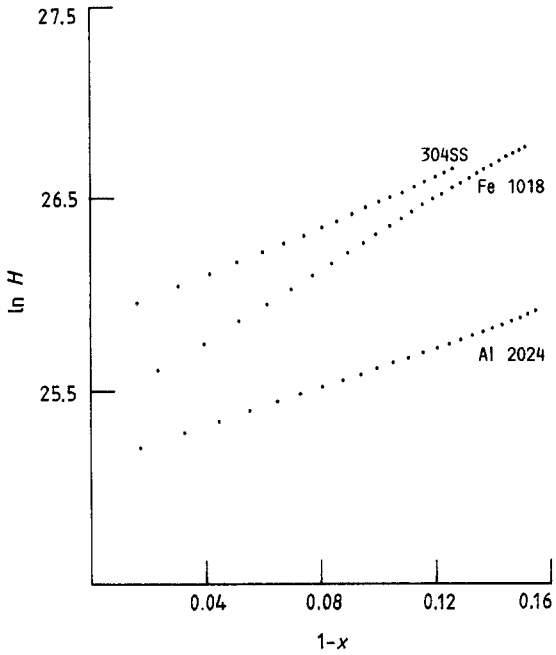

Figure 6. $\ln H$ (from equation (2.13)) versus $(1-x)$ where $x = (V/V_0)^{1/3}$ for several alloys using the shock wave data of [32] and [33].

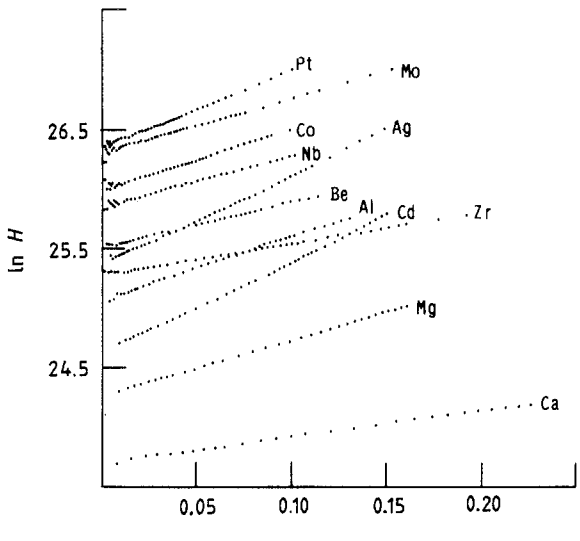

Figure 7. $\ln H$ (from equation (2.13)) versus $(1-x)$ where $x = (V/V_0)^{1/3}$ for several metals using the shock wave data of [34].

by our method, which provides a global fit to the data. Aside from the scatter for small compressions, the plots of $\ln H(x)$ are essentially linear. Values of the fitting parameters, as well as R for the data in this subsection, are found in table 2.

4.4. Ionic crystals

Sodium chloride plays a somewhat singular role among the alkali halides, in that it has long been used as a pressure standard. Consequently its P, V relation is fairly well known

Table 2. Curve-fitting parameters B_0 and B_0' from equation (2.13) for various metals and alloys.

Material	B_0 (10^{11} Pa)	B_0'	R	$(V/V_0)_{min}$
Ag[a]	1.045	6.0	0.9892	0.62
Pt[a]	2.798	5.3	0.998	0.73
Co[a]	1.969	4.3	0.996	0.73
Al[a]	0.764	4.7	0.999	0.66
Nb[a]	1.694	3.9	0.992	0.73
Cd[a]	0.494	6.1	0.9996	0.61
Be[a]	1.200	3.6	0.999	0.70
Mg[a]	0.344	5.1	0.9989	0.66
Ca[a]	0.195	2.5	0.9982	0.47
Nb[a]	1.700	3.9	0.9999	0.61
Mo[a]	2.662	4.1	0.9945	0.53
1018 steel[a]	1.063	7.1	0.997	0.61
Al 2024[a]	0.798	4.5	0.9996	0.60
304 stainless steel[a]	1.662	5.3	0.9995	0.67
Pt[b]	2.775	5.4	0.9997	0.69
Mo[b]	2.685	4.0	0.9999	0.68
Cr[b]	1.887	5.5	0.9994	0.73
Be[b]	1.192	3.5	0.9999	0.68
Zr[b]	0.9294	3.0	1	0.82
Mg[b]	0.3433	4.6	0.9997	0.61

[a] [32, 33].
[b] [34].

for compressions up to the phase transition at $V/V_0 = 0.64$. Figure 8 shows the results of plotting P versus (V/V_0), computed from the measured isotherms of several groups [35–40]. Our fit (table 3) to this compilation of data, using ln H for the isotherm of [32], yields values of $B_0 = 2.36 \times 10^{10}$ Pa and $B_0' = 5.1$. These values are in good agreement with ultrasonic measurements of $B_0 = 2.34 \times 10^{10}$ Pa and $B_0' = 5.35$ [14]. Isotherms ($T = 298$ K) for most of the other alkali halides were taken from the compendium of shock wave results in [34].

Figure 9 shows the plot of ln $H(x)$ versus $(1 - x)$ for alkali halides. All of the results can clearly be fitted by a straight line. However, the plots for RbBr and RbCl show a systematic upward curvature, though the R-values indicate a good linear fit. The origin of this curvature is unknown. Isotherms ($T = 0$ K) for SiC, WC, and MgO were taken from the shock wave data of [32, 33]. The resulting ln $H(x)$ are plotted in figure 10. The linearity of the curves is again clear. The fitting parameters, B_0 and B_0', as well as R, are given in table 3.

4.5. Rare-gas solids

Isothermal compression data were taken from [29] and [30]. Results for Kr, Ar, and Ne are reported at 4.2 K and one other temperature. Results were not available for He. Figure 11 shows the results of plotting ln $H(x)$ for these solids. The fit to a straight line is again evident. Results for B_0, B_0', and R are given Table 4.

Xenon in particular has been studied to somewhat higher compressions using diamond anvil cell techniques. Figure 12 shows a plot of data from [41]. The lower-

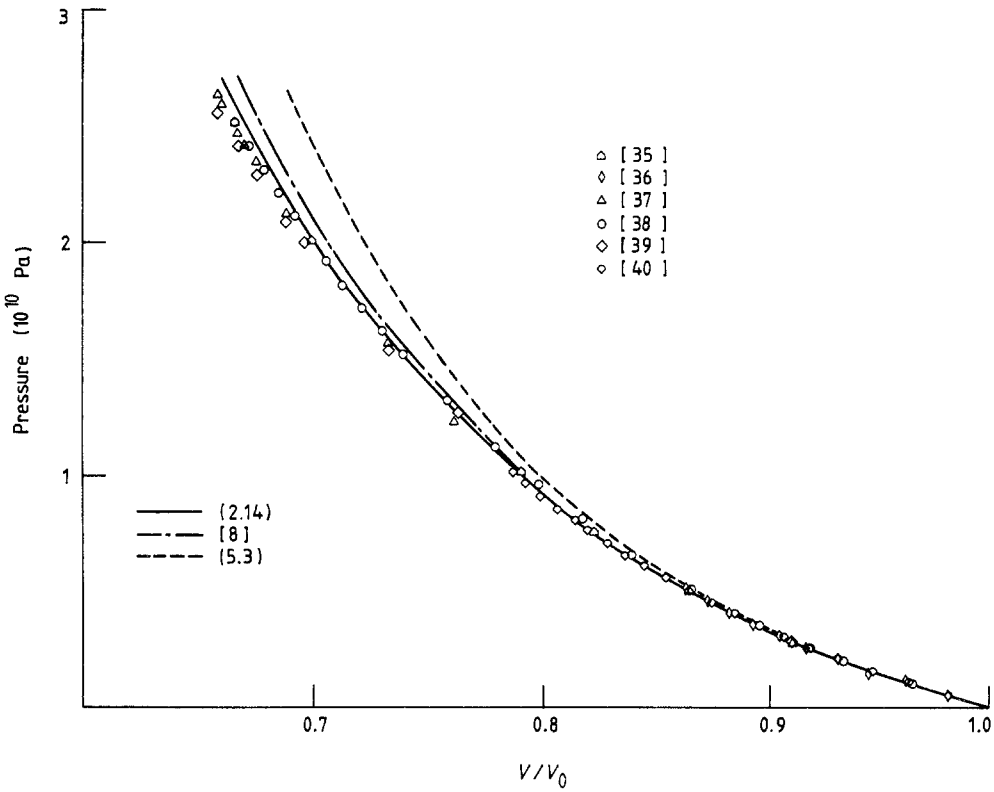

Figure 8. A comparison of pressure versus reduced volume (V/V_0) between the present Murnaghan [43] and Birch equation [8] with NaCl experimental data [35]–[40] for B_0 and B_0' from ultrasonic experiments [4].

Table 3. Curve-fitting parameters B_0 and B_0' from equation (2.13) for the alkali halides and selected covalent solids.

Substance	B_0 (10^{10} Pa)	B_0'	R	$(V/V_0)_{min}$
MgO	15.17	4.8	0.9996	0.70
SiC	20.11	2.6	0.9997	0.70
WC	36.37	4.5	0.9999	0.75
KF	6.245	5.0	0.9996	0.61
NaF	4.687	3.9	0.996	0.82
LiCl	3.268	4.1	0.9991	0.71
NaCl	2.360	5.1	0.9993	0.70
LiBr	2.189	5.5	0.9997	0.65
NaBr	2.083	4.4	0.9996	0.64
NaI	1.981	4.4	0.9999	0.61
RbF	1.487	4.9	0.9998	0.61
KI	0.931	4.7	0.9996	0.57
RbBr	0.757	5.2	0.9993	0.58
RbCl	0.568	6.0	0.9996	0.60

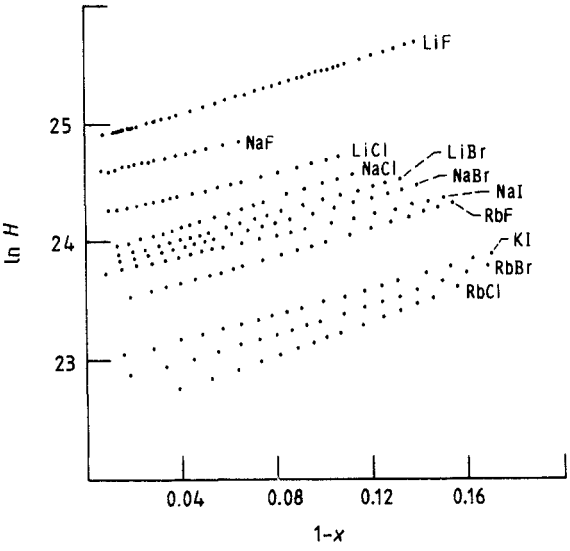

Figure 9. $\ln H$ (from equation (2.13)) versus $(1-x)$ where $x = (V/V_0)^{1/3}$ for several alkali halides for isotherms from [34].

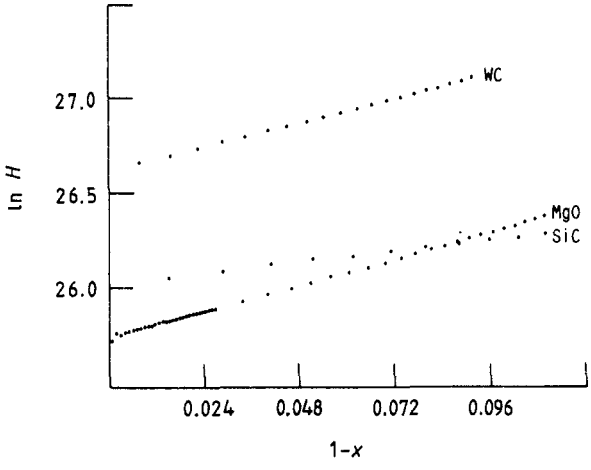

Figure 10. $\ln H$ (from equation (2.13)) versus $(1-x)$ where $x = (V/V_0)^{1/3}$ for WC, MgO, and SiC for the 0 K isotherms of [32] and [33].

Table 4. Curve-fitting parameters B_0 and B_0' from equation (2.13) for the rare gas solids and hydrogen.

Material	B_0 (10^9 Pa)	B_0'	R	$(V/V_0)_{min}$
Ne (4.2 K)	1.080	8.4	0.9999	0.68
Ne (19.9 K)	0.816	8.9	0.9999	0.67
Kr (4.2 K)	3.308	7.8	0.99998	0.79
Kr (77 K)	2.119	8.7	0.9998	0.76
Ar (4.2 K)	2.834	7.8	0.99998	0.78
Ar (77 K)	1.411	9.3	0.99996	0.73
Xe (4.2 K)	3.612	7.9	0.99997	0.80
Xe (159 K)	1.484	9.5	0.99995	0.73
H_2	0.166	7.3	0.9999	0.2
D_2	0.309	7.1	0.9999	0.2
H_2	0.162	7.5	0.9999	0.2
D_2	0.302	7.2	0.9997	0.2

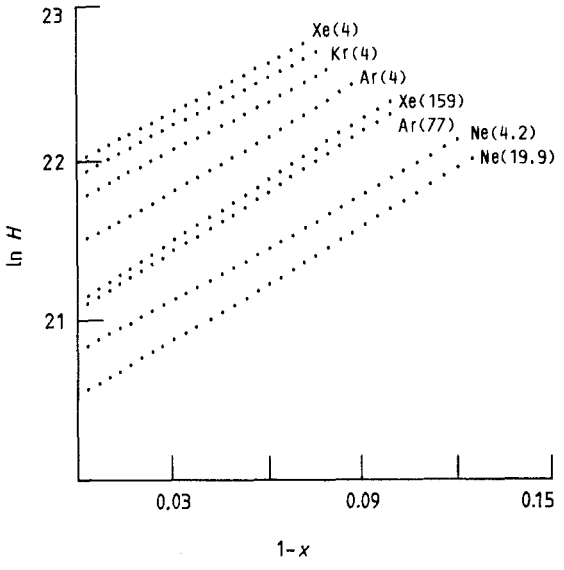

Figure 11. $\ln H$ (from equation (2.13)) versus $(1-x)$ where $x = (V/V_0)^{1/3}$ for rare gas solids for several temperatures (given in K against the element symbol); data from [29] and [30].

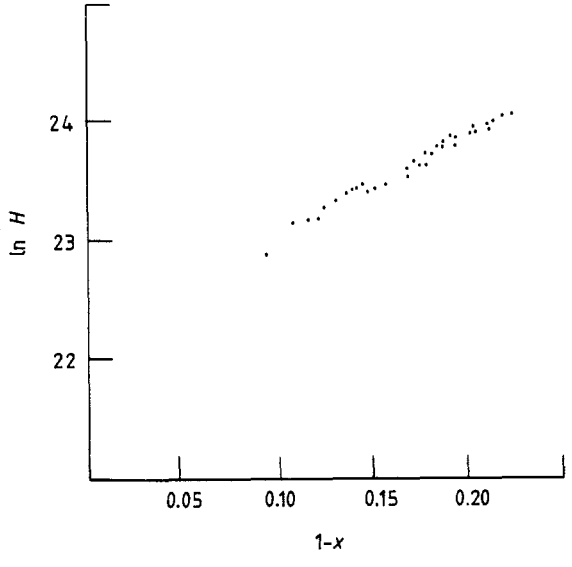

Figure 12. $\ln H$ (from equation (2.13)) versus $(1-x)$ where $x = (V/V_0)^{1/3}$ for xenon at high compression; data from [41].

pressure data of [29] are also reported. The experimental results of [41], provided in table form by Professor Asaumi, have not been smoothed and are rather scattered. They are consistent with the linearity hypothesis but are unable to reveal small deviations from it.

4.6. Some polymers and a glass

Contrary to our general procedures, the results in this subsection definitely represent a selection of the data. Most of the data on polymers (reported in [34] and [42]) had one

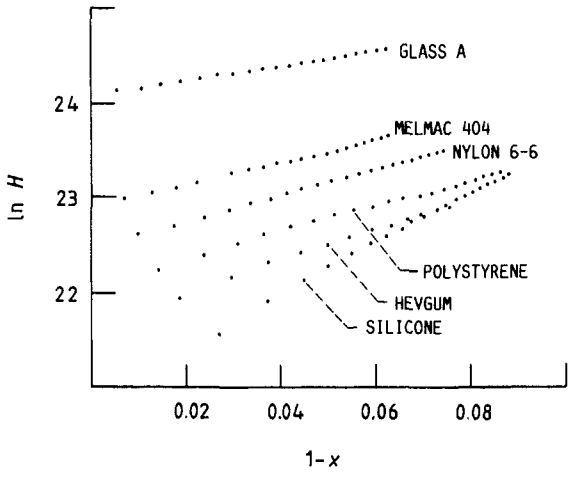

Figure 13. $\ln H$ (from equation (2.13)) versus $(1-x)$ where $x = (V/V_0)^{1/3}$ for some polymers and glass; data from [34] and [42].

Table 5. Curve-fitting parameters B_0 and B_0' from equation (2.13) for some plastics and amorphous solids.

Material	B_0 (10^9 Pa)	B_0'	R	$(V/V_0)_{\min}$
Polystyrene	3.980	10.1	0.9977	0.76
Silicone 160	1.202	19.0	0.9988	0.76
Glass A	29.09	6.2	0.9989	0.83
Nylon 6–6	5.824	10.1	0.9994	0.80
Hevea gum	2.598	12.1	0.9988	0.79
Melmac 404	8.897	8.7	0.991	0.82

or more phase transitions in the region of interest. The data given here are those for which straight lines were obtained. The general utility of our analysis for this group of solids remains unknown. Nonetheless, it seemed so surprising to us, given the complex structure of polymers, that the analysis would work at all for these substances, that we decided to include them in our report.

The isotherms were taken from the results of Bridgman as compiled in [34]. We note that hevea gum is natural rubber. The resulting plots of $\ln H(x)$ are shown in figure 13. The fitting parameters and correlation factor were given in table 5.

5. Is universality trivial?

In the last section, we plotted the isotherms of many solids as $\ln H$ versus $1-x$. The resulting nearly straight lines were taken as evidence for universality. In this section, we discuss some questions concerning the validity of this inference in light of the data.

The basic result is the observation that one can predict isotherms in the absence of phase transitions, given B_0 and B_0'. For small compressions, this statement is trivial, since P can be expressed as a power-series expansion whose lowest-order coefficients are fixed by B_0 and B_0'. If the universal EOS is to be non-trivial, it must make accurate predictions where the truncated power series fails.

The widely used Murnaghan EOS [43] is a power series approach which uses only B_0 and B_0'. Hence we should compare the universal and Murnaghan EOS with experiment.

The Murnaghan EOS is derived by representing B as a power series in P and truncating after the second term,

$$B(P) = B_0 + B_0' P. \tag{5.1}$$

Equation (5.1) can be integrated for P using

$$B = -V(\partial P/\partial V)_T. \tag{5.2}$$

The result is the Murnaghan EOS

$$P(x, T) = B_0(T)(B_0'(T))^{-1}(x^{-3B_0'(T)} - 1). \tag{5.3}$$

From equations (5.1)–(5.3), it is clear that the Murnaghan EOS serves as a convenient test as to how well a truncated power series expression can represent isothermal compression data.

The universal EOS can be used to predict the variation in B as a function of compression. Using (2.4) and (5.2) one obtains

$$B(x, T) = (B_0(T)/x^2)[2 + (\eta(T) - 1)x - \eta^2(T)x^2]\exp[\eta(T)(1 - x)]. \tag{5.4}$$

This expression can be compared with (5.1) using (5.3).

Anderson and Swenson [29] have reported $P(V)$ and $B(V)$ for compressions greater than 50% for H_2 at $T = 4.2$ K. In figure 14(*a*) we plot their results together with predictions of the universal and Murnaghan EOS [43]. The values of $B_0 = 1.7 \times 10^9$ Pa and $B_0' = 7$ are taken from [29]. As can be seen, the universal expression is very markedly superior to the Murnaghan expression for compressions, V/V_0, greater than 0.80. Figure 14(*b*) shows a similar result for the bulk modulus. A similar result is obtained for NaCl (figure 8). In this case, $B_0 = 2.34 \times 10^{10}$, and $B_0' = 5.35$ were taken from ultrasonic experiments. In this case we compare also to the Birch equation [8] another two parameters (B_0, B_0') widely used in the EOS literature. As is shown in figure 8, the universal EOS is in good agreement while the Murnaghan expression again deviates for compressions greater than 0.80. Similar results were obtained for each class of solid. The Birch equation has a better agreement than the Murnaghan and is slightly worse than the present model.

Consequently, we conclude that the universal EOS accurately includes the non-linear physics (WRT (5.1)). Note that we do not imply by these comparisons that the universal relation is superior to all other ways of fitting isothermal P, V curves; rather, we have shown that it includes the non-linear physics with sufficient accuracy to be useful for data analysis and data extrapolation (e.g., the NaCl data just discussed) purposes. Most importantly, we have shown that there is a universal form for the EOS of *all* classes of solid.

In the paper we have primarily compared the Murnaghan and universal equations of state for the reasons given above. However, we remark that recent work [44] shows that the universal EOS is a more accurate representation of the data for the entire range at B_0, B_0' and x encountered experimentally than the Birch equation [8], the work reported, in [45] as well as some more recent work [46].

The ln H curves of § 4 are a rather indirect way of checking if equation (2.14) can describe experimental isotherms. Figure 15(*a–d*) shows pressure-reduced volume plots of experimental isotherms along with curve fits to the universal EOS fit for natural rubber

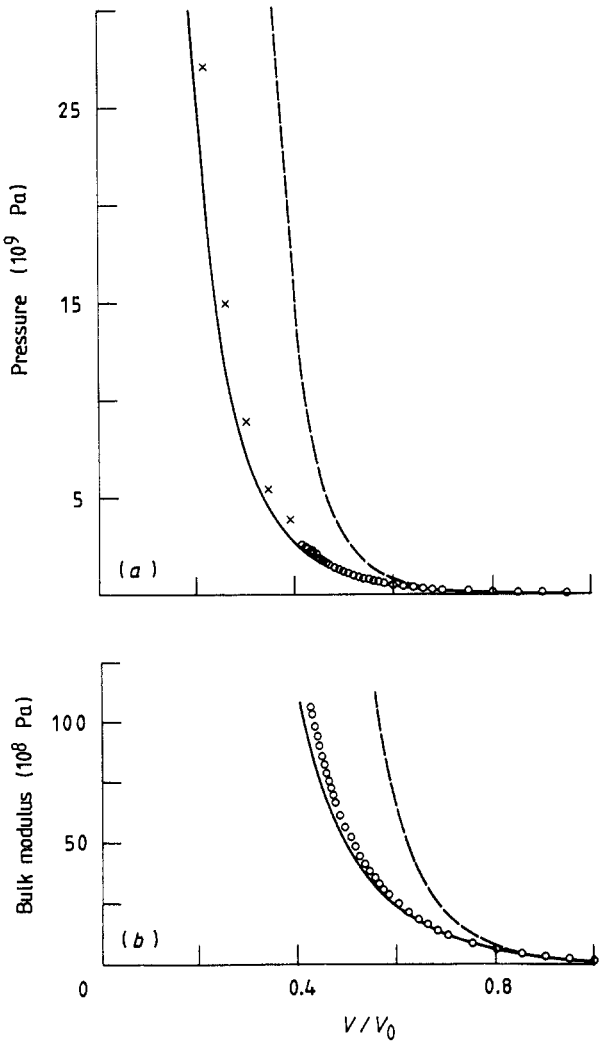

Figure 14. A comparison for hydrogen between the Murnaghan expression ([43], broken curve) and the present model (universal relation, full curve) showing the effects of non-linear terms. B_0 and B_0' for theoretical curves were obtained from [30] (*a*) Pressure versus reduced volume, V/V_0, (*b*) Bulk modulus versus reduced volume, V/V_0, (Experimental data: ○, [30], ×, [2].

(hevea gum), Cs, Mo, and Xe. The fits are uniformly excellent. The fitting parameters are taken from § 4.

Since the universal EOS accurately contains the non-linear portions of the EOS, we can use it to examine these non-linearities. Figure 16 shows a plot of B/B_0 versus P/B_0 for the hydrogen data of [29]. The broken line is the linear extrapolation (equation (5.1)). The full line represents the universal EOS and does a good job of representing the data up to compressions as large as 0.45. Finally, equations (5.4) and (5.2) can be used to calculate the higher-pressure derivatives of B. One finds explicitly for the second derivative

$$B_0 B_0'' = B_0(T)(\partial^2 B/\partial P^2)_{T,P=0} = \tfrac{19}{36} - \tfrac{1}{2}B_0' - \tfrac{1}{4}(B_0')^2. \tag{5.5}$$

A discussion of higher-order derivatives as well as a general analysis of the universal EOS and its application to other physical properties can be found in [47].

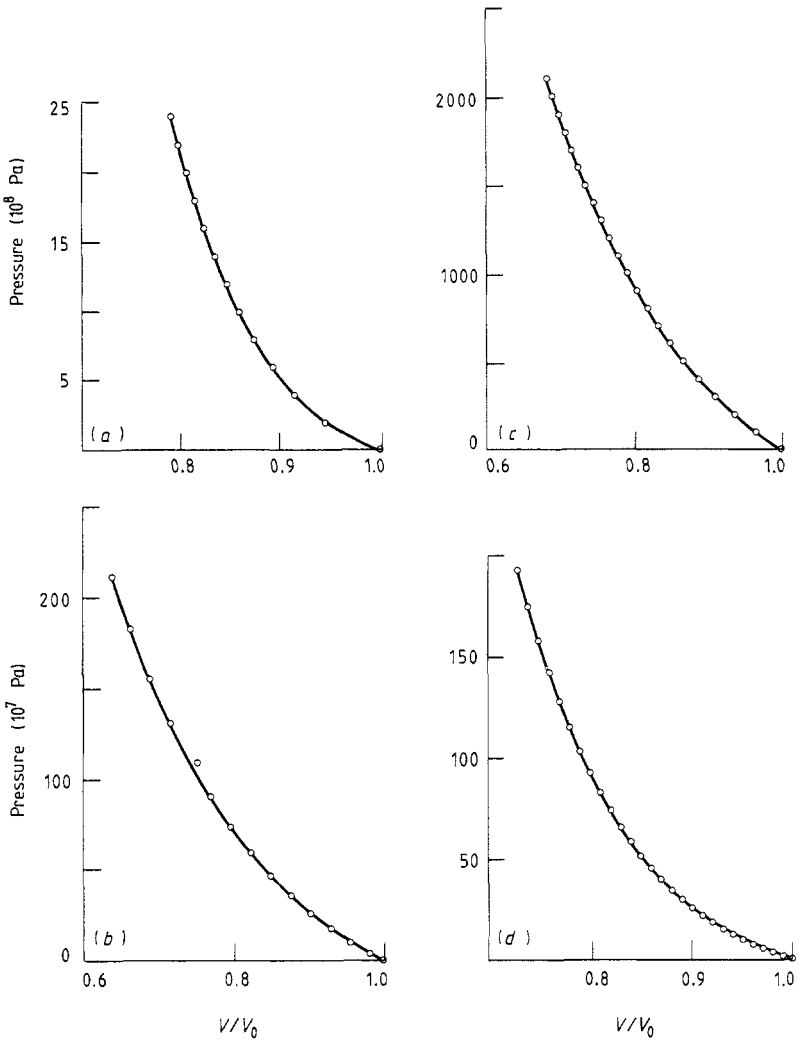

Figure 15. Pressure versus reduced volume plots of experimental data and a fit to the present model (equation (2.14)) for (*a*) natural rubber (hevea gum) [32], [34]; (*b*) Cs [22], [28]; (*c*) Mo [32], [33] and (*d*) Xe [31].

6. Universality and data analysis

The technique of plotting isotherms as $\ln H(x)$ versus $1 - x$ illuminates the common features of the equation of state of solids. As we discuss below, this method is particularly sensitive to certain errors in the data. In addition, by concentrating on $\ln H(x)$ and the inter-particle spacing (which is proportional to x), one treats the low- and high-pressure data on an equal footing. Consequently, it seems to us that, for many purposes, plots of the isotherm as $\ln H(x)$ versus $1 - x$ might become a standard method of data analysis.

First, we remark that the analytic from of (2.14) was introduced as an approximate representation. For sufficiently high pressures and sufficiently accurate measurements non-linearities in plots of $\ln H$ versus $1 - x$ may become apparent. In particular, one might find a small systematic curvature in the data at *large* $1 - x$. If the deviations

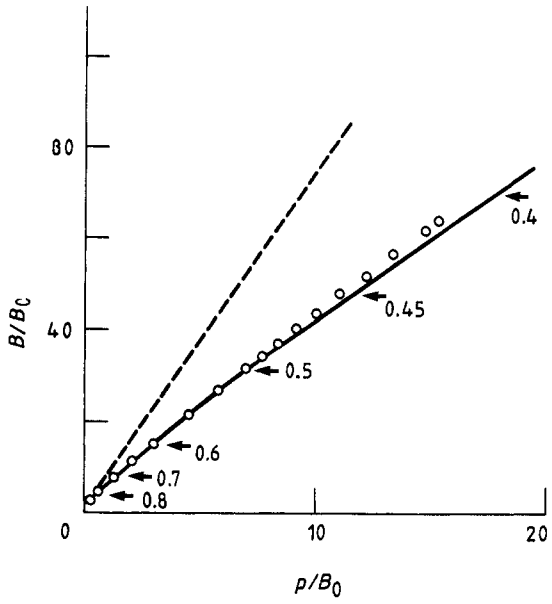

Figure 16. A plot of the bulk modulus (B/B_0) versus pressure (P/B_0) for the hydrogen data of [29] (open circles) showing the nonlinear contributions by comparing the present model (full curve) with the Murnaghan equation [43] (broken line). B_0 and B_0' were obtained by fitting to equation (2.14). The arrows indicate values of V/V_0.

from linearity are smoothly varying, we recommend fitting the resulting curve with a polynomial, i.e.

$$\ln H(x) = \ln B_0 + \eta(1-x) + \beta(1-x)^2 + \gamma(1-x)^3 + \ldots . \tag{6.1}$$

The corresponding pressure–volume curve is

$$P(x) = [3B_0(1-x)/x^2] \exp[\eta(1-x) + \beta(1-x)^2 + \gamma(1-x)^3 + \ldots]. \tag{6.2}$$

We note that β appears in the calculation of the second pressure derivative of the bulk modulus at zero pressure while γ appears in the third. Finally, the results of the last section indicate that β and γ in most cases are small and the determination of their values will require very careful measurements over a wide range of compression. One exception is a U–Mo alloy that is discussed below.

Various forms of error are clearly emphasised with ln H plots. For example, in figure 7 the data tend to scatter for small $1-x$, and figure 12 shows unsmoothed data for xenon. The lack of any systematic trend in the scatter in figure 7 indicates that it is likely due to lack of sufficient accuracy in the reported isotherms at low compressions. An extensive data analysis showing these effects for materials of geophysical interest is presented in [48].

A well known difficulty in obtaining reliable isotherms is the determination of the zero-pressure volume, V_0. Such errors leave a very clear signature on a ln H plot, namely, the plot becomes curved for *small* $1-x$. Figure 17 shows the results of errors of ± 1 and $\pm 5\%$ in V_0 using values of B_0 and B_0' for NaCl [14]. As an example, data from the literature for NaCl which has a curved ln H plot for small $1-x$ are presented in figure 18. This curvature is explained as an error in V_0. Decker [49] predicted high-temperature isotherms for NaCl based on measured values at 25 °C. In these extrapolations, the value of V_0 at 25 °C is used at the higher temperatures. His extrapolated isotherm for $T =$ 500 °C is shown in figure 18. The curvature suggests that the value V_0 in computing the isotherm is too small. We have replotted these data in the insert with a value for V_0 that

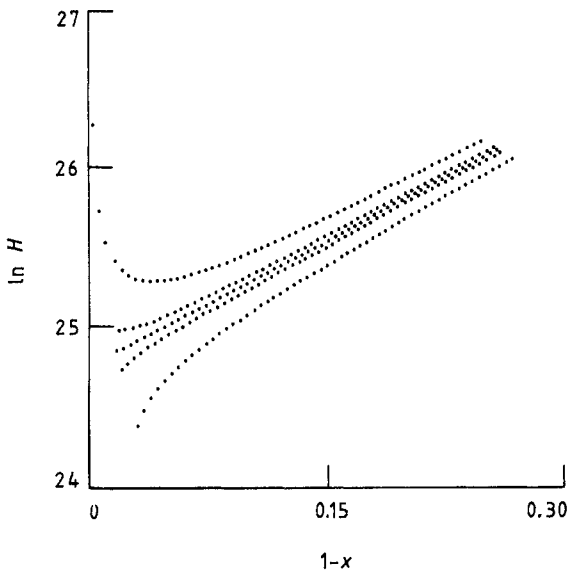

Figure 17. A plot of $\ln H$ (from equation (2.13)) versus $(1-x)$ where $x = (V/V_0)^{1/3}$ showing the effects of ± 1 and $\pm 5\%$ errors in V_0, the equilibrium volume, on $\ln H$ plots using B_0 and B_0' from ultrasonic data for NaCl [4].

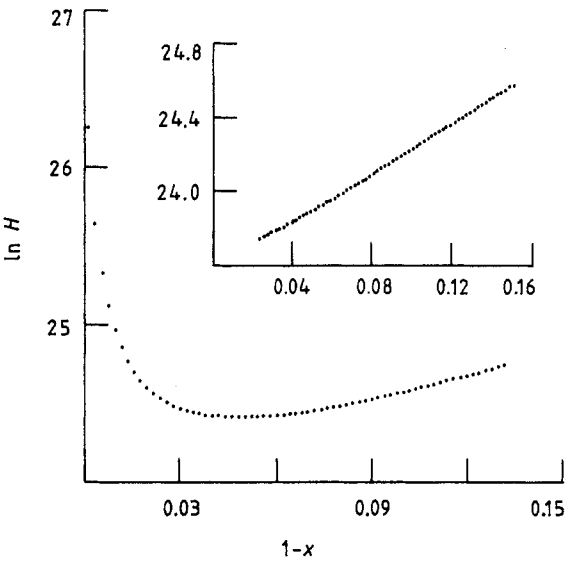

Figure 18. A plot of $\ln H$ (from equation (2.13)) versus $(1-x)$ where $x = (V/V_0)^{1/3}$ of a 500 °C isotherm from [49] using the 25 °C value for V_0. The inset shows the result of replotting the curve with $V_0' = 1.068\,V_0$.

removes the curvature (~6.8%) (comparing with the value at the thermal expansion for NaCl at 500 °C in the literature +6.8% [50]); we see that the curvature can be plausibly explained as resulting from the use of the value of V_0 at 25 °C rather than that at 500 °C. We should point out that a second type of error is possible. If V_0 is known correctly but $\Delta V = V_0 - V$ is systematically in error by a fixed percentage, then no significant signature is found in the $\ln H$ plot. Consequently, small errors will propagate in determining B_0 and B_0'.

Our basic observation is that $\ln H$ plots are linear in the absence of phase transitions. It is of considerable interest for purposes of data analysis to show a case where a phase

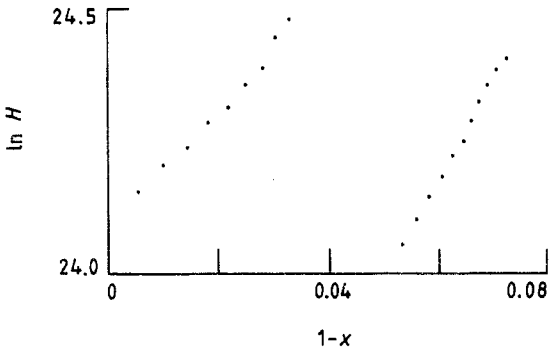

Figure 19. A plot of $\ln H$ (from equation (2.13)) versus $(1-x)$ where $x = (V/V_0)^{1/3}$ for phosphorous [40], [42] showing the effects of a phase change.

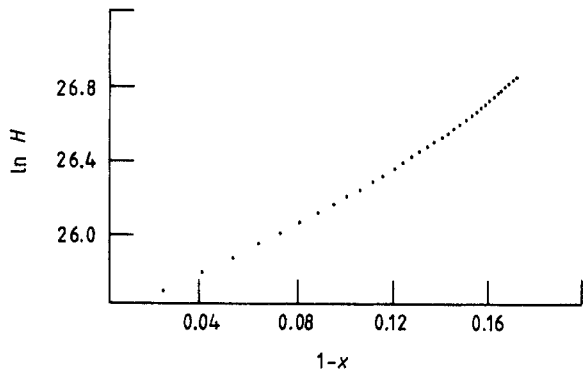

Figure 20. A plot of $\ln H$ (from equation (2.13)) versus $(1-x)$ where $x = (V/V_0)^{1/3}$ for a U–Mo alloy [32] isotherm showing a curvature which cannot be explained in the present model.

transition does occur. In figure 19 the $\ln H$ plot is shown for phosphorous. There is an abrupt, discontinuous change in the curve at the $1-x$ value, which marks a phase transition. Jakobson and Vinet have applied this analysis with success to solidification transformations in liquid lubricants at elevated pressures [51].

Figure 20 shows a $\ln H$ plot of U–Mo alloy [32] where the isotherm was inferred from shock wave data. There is a definite curvature in the data at large $1-x$. This curvature cannot be explained by an incorrect V_0, which introduces curvature only at small $1-x$. The origin of the curvature is unknown. However, one possibility is that a continuous change in the electronic ground state of the alloy is occurring.

As discussed earlier, the significance of the linearity of $\ln H$ plots can be assessed by comparing them to the results of using the Murnaghan EOS. Another way of assessing the universal EOS is to use them to extract B_0 and B_0' for a typical isotherm. The Murnaghan EOS is designed to be most accurate at low pressures. Consequently, we have extracted B_0 and B_0' using the two different methods with a variable number of data points. Higher pressures are included as the number of points increases. The results are shown in table 6 for NaCl. As can be seen, the values of B_0 and B_0' extracted from the $\ln H$ plots are almost constant as the number of points increases. More importantly, there are in good agreement with the measured ultrasonic values. On the other hand, the values of B_0 and B_0' extracted using the Murnaghan EOS vary with the number of data points. For a small number of points (low-pressure data), the values of B_0 and B_0' extracted using Murnaghan's EOS agree well with experiment. For more points, the agreement becomes progressively poorer. Consequently, even in those cases where the

Table 6. Comparison of fitting parameters between present EOS and the Murnaghan model as a function of number of points used in fitting for NaCl.

Number of points	Present		Murnaghan	
	B_0 (10^{10} Pa)	B_0'	B_0 (10^{10} Pa)	B_0'
8	2.36	5.16	2.37	4.86
15	2.36	5.03	2.38	4.67
25	2.36	5.03	2.38	4.53
45	2.36	5.08	2.44	4.27
69	2.35	5.15	2.54	4.00

Murnaghan EOS can be fit to a broad range of data, the resulting determinations of B_0 and B_0' may be expected to yield values that disagree with low-pressure values, whereas the universal EOS allows a stable determination of B_0 and B_0' using the entire range of measured data.

7. Summary

It has been shown in this paper that the EOS of solids can be expressed in terms of a universal function. It was first argued on theoretical grounds that such a universal relation ought to exist. Next the universal relation was exhibited and its form determined from the measured isotherms for many solids. Finally, it was suggested that the universal method might provide a potentially suitable basis for data analysis.

Acknowledgment

One of us (PV) would like to thank the French 'Ministere des Relations Exterieures' for financial support. The Ames Laboratory is operated for the US Department of Energy by Iowa State University under contract No W-7405-ENG-82, and this work was supported by the Director of Energy Research, US Office Basic Energy Sciences.

References

[1] Godwal B K, Sikka S K and Chidambaram R 1983 *Phys. Rep.* **102** 121
[2] Van Straaten J, Wijngaarden R J and Silvera I F 1982 *Phys. Rev. Lett.* **48** 97
[3] Dass N and Kumari M 1985 *Phys. Status Solidi* B **127** 103
[4] Ruoff A L and Chhabildas L C 1978 *High Pressure-Science and Technology, Sixth AIRAPT Conference* vol 1, ed. K D Timmerhaus and M S Barber (New York: Plenum) pp 19–32
MacDonald J R 1969 *Rev. Mod. Phys.* **41** 316
[5] Zharkov V N and Kalinin V A 1971 *Equations of State for Solids at High Pressures and Temperature* (New York: Plenum Consultants Bureau)
[6] Holian K S (ed.) 1984 *T-4 Handbook of Material Properties Data Bases, vol 1C: Equations of State* Los Alamos Report No LA-10160-MS UC-34
[7] Barnes J 1967 *Phys. Rev.* **153** 269
[8] Birch F 1952 *J. Geophys. Res.* **457** 227
[9] Torrens I M 1972 *Interatomic Potentials* (New York: Academic)
[10] Vinet P, Ferrante J, Smith J R and Rose J H 1986 *J. Phys. C: Solid State Phys.* **19** L467

[11] Rose J H, Ferrante J and Smith J R 1981 *Phys. Rev. Lett.* **47** 675
[12] Smith J R, Ferrante J and Rose J H 1982 *Phys. Rev.* B **25** 1419
[13] Ferrante J, Smith J R and Rose J H 1983 *Phys. Rev. Lett.* **50** 1385
[14] Rose J H, Smith J R and Ferrante J 1983 *Phys. Rev.* B **28** 1935
[15] Guinea F, Rose J H, Smith J R and Ferrante J 1984 *Appl. Phys. Lett.* **44** 53
[16] Rose J H, Smith J R, Guinea F and Ferrante J 1984 *Phys. Rev.* B **29** 2963
[17] Smith J R, Rose J H, Ferrante J and Guinea F 1984 *Many-Body Phenomena at Surfaces* ed. D Langreth and H Suhl (New York: Academic) p 159
[18] Ferrante J and Smith J R 1985 *Phys. Rev.* B **31** 3427
[19] Smith J R and Ferrante J 1985 *Mater. Sci. Forum* **4** 21
[20] Rose J H, Vary J P and Smith J R 1981 *Phys. Rev. Lett.* **50** 1385
[21] Gordon R G and Kim Y S 1976 *Phys. Rev.* B **14** 4593
[22] Anderson M S and Swenson C A 1985 *Phys. Rev.* B **31** 668
[23] Vinet P, Smith J R, Ferrante J and Rose J H 1987 *Phys. Rev.* B **35** 1945
[24] Swenson C A 1968 *J. Phys. Chem. Solids* **29** 1337
[25] Anderson M S and Swenson C A 1975 *J. Phys. Chem. Solids* **36** 145
[26] Anderson O L, Boehler R and Sumino Y 1982 *High Pressure Research in Geophysics* ed. A Akimoto and M H Manghani (Tokyo: Centre for Academic Publications) p 273
[27] Packard J R and Swenson C A 1963 *J. Phys. Chem. Solids* **24** 1405
[28] Anderson M S and Swenson C A 1983 *Phys. Rev.* B **28** 5395
[29] Anderson M S and Swenson C A 1974 *Phys. Rev.* B **10** 5184
[30] Anderson M S, Fugate R Q and Swenson C A 1973 *J. Low Temp. Phys.* **10** 345
[31] Spiegel M R 1961 *Theory and Problems of Statistics* (New York: Schaum) p 241
[32] McQueen R G, Marsh S P, Taylor J W, Fritz J N and Carter W J 1976 *High-Velocity Impact Phenomena* ed. R Kinslow (New York: Academic)
[33] Carter W J, Marsh S P, Fritz J N and McQueen R G 1971 *Accurate Characterization of the High Pressure Environment* Special Publication No 326, ed. E C Lloyd (Washington, DC: NBS) p 147
[34] Kennedy G C and Keeler R N 1972 *American Institute of Physics Handbook* 3rd edn, ed. D E Gray (Nerw York: McGraw-Hill) pp 4–38
[35] Perez-Albuerne E A and Drickamer H G 1965 *J. Chem. Phys.* **43** 1381
[36] Vaidya S N and Kennedy G C 1971 *J. Phys. Chem. Solids* **32** 951
[37] Weaver J S, Takahashi T and Bassett W A 1971 *Accurate Characterization of the High Pressure Environment* Special Publication No 326, ed. E C Lloyd (Washington, DC: NBS) p 189
[38] Fritz J N, Marsh S P, Carter W J and McQueen R G 1971 *Accurate Characterization of the High Pressure Environment* Special Publication No 326, ed. E C Lloyd (Washington, DC: NBS) p 201
[39] Thomsen L 1970 *J. Phys. Chem. Solids* **31** 2003
[40] Bridgman P W 1945 *Proc. Am. Acad. Arts Sci.* **76** 1
[41] Asaumi K 1984 *Phys. Rev.* B **29** 7026
[42] Bridgman P W *The Physics of High Pressure* 1949 (London: Bell)
[43] Murnaghan F D 1951 (New York: Wiley)
[44] Schlosser H and Ferrante J private communication
[45] Grover R, Getting I C and Kennedy G D 1973 *Phys. Rev.* B **7** 567
[46] Dodson B W 1987 *Phys. Rev.* B **35** 2619
[47] Vinet P 1986 *PhD Thesis* Ecole Centrale de Lyon
[48] Vinet P, Ferrante J, Rose J H and Smith J R 1987 *J. Geophys. Res.* **92** 9319
[49] Decker D L 1971 *J. Appl. Phys.* **42** 3239
[50] Touloukian Y S, Kirby R K, Taylor R E and Lee T Y R 1977 *Thermophysical Properties of Matter vol 13* (New York: IFI Plenum) p 1011
[51] Jakobson B O and Vinet P 1987 *Trans. ASME J. Tribol.* **109** 709